ACCSCIENCE PUBLISHING

Asian Journal of Water, Environment and Pollution

ORIGINAL RESEARCH ARTICLE

Solidification of river sediment by mayenite and biochar composite stabilizers: Strength development, microstructural evolution, and leaching behavior

Wenhao Li[1,2], Yalin Yu[3], Haoyuan Zhang[3], Ning Fang[1,2]*, Xiankai Wang[1], Shouqiang Huang[3], and Dongdong Ge[3,4]*

[1]China Three Gorges Corporation, National Engineering Research Center of Eco-Environment in the Yangtze River Economic Belt, Wuhan, China

[2]Shanghai Investigation, Design & Research Institute Co., Ltd., Shanghai, China

[3]School of Resources and Environmental Engineering, Jiangsu University of Technology, Changzhou, China

[4]Shanghai Engineering Research Center of Solid Waste Treatment and Resource Recovery, School of Environmental Science and Engineering, Shanghai Jiao Tong University, Shanghai, China

***Corresponding authors:**
Ning Fang
(fang_ning@ctg.com.cn);
Dongdong Ge
(ddge1118@sjtu.edu.cn)

Citation: Li W, Yu Y, Zhang H, *et al*. Solidification of river sediment by mayenite and biochar composite stabilizers: Strength development, microstructural evolution, and leaching behavior. *Asian J Water Environ Pollut*. 2026;23(5):026300202. doi: 10.36922/AJWEP026300202

Received: July 20, 2026

Revised: August 15, 2026

Accepted: August 21, 2026

Published online: September 7, 2026

Copyright: © 2026 Author(s). This is an Open-Access article distributed under the terms of the Creative Commons Attribution License, permitting distribution, and reproduction in any medium, provided the original work is properly cited.

Publisher's Note: AccScience Publishing remains neutral with regard to jurisdictional claims in published maps and institutional affiliations.

Abstract

The resource utilization of urban river sediments is often hindered by their high-water content, poor mechanical properties, and potential environmental risks. In this study, a composite stabilization system based on mayenite (CA) and coconut-shell biochar (BC) was developed to simultaneously improve the engineering performance and environmental safety of contaminated sediments. The effects of initial water content, CA dosage, CA particle size, BC dosage, and BC particle size were systematically investigated using unconfined compressive strength (UCS) tests. The optimal conditions were 70% initial water content, 40% CA (250 mesh), and 20% BC (200 mesh), achieving a maximum UCS of 2.31 ± 0.11 MPa. Microstructural analyses revealed distinct functional roles of the two stabilizers. CA primarily provided mechanical stabilization by forming cementitious hydration products that bound sediment particles into a dense, continuous matrix, whereas BC mainly enhanced environmental stabilization through pore refinement and adsorption-assisted contaminant retention. As a result, the CA–BC composite significantly reduced the leaching of heavy metals, chemical oxygen demand, total nitrogen, and total phosphorus compared to CA stabilization alone. This study demonstrates that CA and BC play complementary roles in sediment stabilization, with CA dominating mechanical reinforcement and BC enhancing environmental stability, providing an effective strategy for the sustainable reuse of dredged sediments in geotechnical engineering.

Keywords: Urban river sediment; Mayenite; Biochar; Stabilization; Unconfined compressive strength

1. Introduction

Large quantities of urban river sediment are continuously generated worldwide due to routine dredging operations, river channel maintenance, and the remediation of black-odorous water bodies.[1-3] Driven by rapid urbanization and growing efforts to restore aquatic ecosystems, the volume of dredged sediment has increased substantially, creating significant challenges for safe disposal and sustainable management. In China, approximately 160 million m^3 of dredged sediment is generated annually from urban river regulation and water environment improvement projects.[4] Similar challenges have been reported globally; for example, more than 50 million tons of marine sediment are dredged annually from ports in France,[2] while the annual dredged sediment quantities reach approximately 400 million tons in the United States and 40 million m^3 in the Netherlands.[5] However, the direct reuse of these sediments in engineering applications is often hindered by their high water content, poor mechanical strength, and high compressibility.[6-9] Cino *et al.*[10] incorporated superabsorbent polymers into dredged marine sediments to reduce pore water content, enabling the resource utilization of the sediments. Mastoi *et al.*[11] treated dredged sediment slurry with ground granulated blast furnace slag and flocculants to improve mechanical dewatering efficiency, thereby increasing the strength of the solidified sediment slurry. Moreover, the coexistence of organic matter, nutrients, and heavy metals may pose potential environmental risks through contaminant migration during disposal or reuse processes.[12-15] Therefore, developing effective stabilization strategies that can simultaneously improve engineering performance and environmental safety is essential for the sustainable management and resource utilization of dredged sediments.

Cementitious binders, including Portland cement, lime, and other calcium-based materials, have been extensively employed for sediment stabilization because hydration reactions generate cementitious products that enhance particle bonding, increase strength, and reduce compressibility.[16,17] Recently, calcium aluminate-based binders have attracted increasing attention due to their rapid hydration kinetics and the formation of calcium-containing hydration products, such as calcium silicate hydrates (C–S–H), calcium aluminosilicate hydrates (C–A–S–H), and ettringite (AFt), which contribute to matrix densification and strength development.[18-20] In particular, mayenite ($Ca_{12}Al_{14}O_{33}$, hereafter referred to as CA), a highly reactive calcium aluminate phase, has shown promising potential as a stabilizing agent owing to its unique hydration characteristics and ability to promote the formation of cementitious phases.[21] Nevertheless, the stabilization efficiency of calcium-based binders remains strongly influenced by sediment properties, including water content, binder dosage, and particle size distribution, especially for soft sediments with high moisture content.

In recent years, biochar has increasingly been incorporated into cementitious systems as a functional additive because its porous structure, high specific surface area, and abundant oxygen-containing functional groups facilitate pore refinement, contaminant adsorption, and microstructural regulation.[22,23] Among biochar types, coconut-shell biochar has attracted particular interest because of its abundant raw materials, low cost, and favorable physicochemical properties.[24,25] However, biochar alone generally exhibits limited cementation capacity and cannot provide sufficient mechanical reinforcement. Therefore, coupling biochar with calcium-based binders may provide a promising strategy by combining the cementitious effect of hydration products with the adsorption and pore-modifying capabilities of biochar. Despite this potential, the synergistic interactions between biochar and calcium aluminate binders during sediment stabilization remain insufficiently understood.

Although calcium aluminate and biochar exhibit complementary advantages, several critical issues remain unresolved. First, the combined effects of key influencing factors, including initial water content, binder dosage, and particle size, on the stabilization performance of calcium aluminate–biochar systems have not been systematically evaluated. Second, the mechanisms governing the interactions between hydration products and biochar in terms of pore structure evolution, strength enhancement, and contaminant immobilization require further clarification. Third, previous studies have mainly focused on mechanical improvement, whereas the coupling relationship between mechanical performance and long-term environmental safety has received comparatively limited attention.

Therefore, we developed a mayenite–biochar composite stabilization system to treat and resource-utilize urban river sediment. The effects of initial water content, mayenite dosage, mayenite particle size, biochar dosage, and biochar particle size on unconfined compressive strength (UCS) were systematically investigated to determine the optimal stabilization conditions. Subsequently, X-ray diffraction (XRD), Fourier transform infrared spectroscopy (FTIR), scanning electron microscopy (SEM), and energy-dispersive X-ray spectroscopy (EDX) analyses were conducted to reveal the microstructural evolution and underlying stabilization mechanisms. Furthermore, leaching tests for heavy metals, chemical oxygen demand (COD), total nitrogen (TN), and total phosphorus (TP)

were performed to evaluate the environmental safety of the stabilized sediment (SS). This study provides new insights into the synergistic stabilization mechanism of mayenite and biochar and offers a practical approach for the sustainable reuse of dredged urban river sediments.

2. Materials and methods

2.1. Raw materials

River sediment used in this study was collected from an urban river channel in Suzhou, China. The sampled sediment was dark gray, highly plastic, and rich in fine particles, with clay and silt as the dominant fractions. After collection, visible debris, plant residues, and gravel were manually removed. The sediment was then homogenized and stored in sealed polyethylene containers prior to use. Based on the source studies, the sediment exhibited high water retention, low structural strength, and poor engineering stability, making it a representative material for solidification/stabilization research. The basic properties of the sediment are shown in Table 1.

The mineral stabilizer, CA ($Ca_{12}Al_{14}O_{33}$), was prepared using analytical-grade calcium oxide (CaO) and aluminum oxide (Al_2O_3) (Sinopharm Chemical Reagent Co., Ltd., China). The CaO and Al_2O_3 were thoroughly mixed according to the predetermined stoichiometric ratio and subsequently calcined in a muffle furnace at 1,200 °C for 4 h to obtain the mayenite stabilizer. After cooling the calcined product to room temperature, it was crushed, ground, and sieved to obtain various particle-size fractions for subsequent tests.

Coconut shell biochar (BC) was selected as the carbonaceous amendment because of its porous structure, high specific surface area, and abundant surface functional groups. The biochar was supplied as a commercial powder (Luoyang Bailian Environmental Protection Technology Co., Ltd., China) and then sieved into different particle-size fractions before use.

2.2. Experimental design

First, experiments on sediment with different moisture contents (40–80%, covering the moisture range commonly encountered in dredged river sediment) and different CA dosages (25–50%, expressed as the mass ratio of stabilizing agent to wet sediment mass) were performed. The UCS of specimens cured for seven days was used as the index to assess the effects of initial sediment water content and CA dosage on SS strength. Secondly, based on the optimum initial sediment water content and CA dosage obtained from the above tests, BC was introduced to form a CA–BC composite stabilizer, and the effects of BC dosage and BC particle size on sediment stabilization were systematically investigated. Then, XRD, FTIR, and SEM–EDX were employed to clarify the microscopic mechanism of strength development by analyzing the hydration products and microstructure. Finally, leaching tests were conducted to evaluate the ability of CA–BC–SS to immobilize heavy metals, thereby assessing its engineering properties and environmental safety.

Table 1. Basic physical and mechanical properties of the raw sediment

Properties	Value
Gravel (%)	0.00
Sand (%)	1.12
Silt and clay (%)	98.90
Liquid limit (%)	64.80
Plastic limit (%)	37.90
Plasticity index (%)	26.90
Maximum dry density (g/cm^3)	1.42
Initial water content (%)	87.40

2.3. Specimen preparation

Sediment was first oven-dried at 60 °C and then weighed according to the designed mix proportion. Deionized water was added to adjust the moisture content to the target value, and the mixture was mechanically stirred to obtain a homogeneous sediment paste. CA was then added according to the designed dosage and mixed thoroughly with the sediment. The mixture was cast into cylindrical acrylic molds (Φ50 mm × 50 mm) in several layers, and each layer was compacted by vibration to minimize entrapped air and improve specimen uniformity. After molding, the specimens were kept in the molds for 24 h, demolded, and then cured in a standard curing box under the designated curing conditions (temperature: 20 ± 2 °C, humidity: 95%) for seven days. The silt samples solidified with CA are denoted as $CA_{x\%}$–SS, where x% represents the CA dosage based on the sediment dry mass.

For the CA–BC composite stabilization system, CA and BC were first dry-mixed thoroughly and then added to the sediment paste. The subsequent mixing, molding, demolding, and curing procedures were identical to those used for the CA-stabilized specimens. The silt samples solidified with CA and BC are denoted as $CA_{x\%}$–$BC_{y\%}$–SS, where x% and y% represent the CA and BC dosages,

respectively, both calculated based on the dry mass of the sediment.

2.4. Unconfined compressive strength test

Cylindrical specimens (Φ50 mm × 50 mm) were prepared, with three parallel specimens for each mixture. After seven days of curing, the specimens were tested using a universal compression testing machine (3,400, Instron, USA) with a load capacity of 50 kN and a displacement measurement accuracy of 0.5 μm. The loading rate was set to 1 mm/min, and the specimens were continuously loaded until failure. The peak stress was taken as the UCS value, and the average value of the three parallel specimens was used for analysis. The UCS results were used to evaluate the effects of initial sediment water content, CA dosage, CA particle size, BC dosage, and BC particle size on SS strength development.

2.5. Leaching tests

The leaching test was conducted in accordance with HJ/T 299–2007, Solid Waste—Extraction Procedure for Leaching Toxicity—Sulphuric Acid and Nitric Acid Method.[26] After the UCS test, the inner portion of the fractured specimens was collected as the leaching sample. The extraction solution was added according to the standard procedure, and the samples were shaken for 20 h. The leachates were then filtered and collected for chemical analysis. Two categories of pollutants were analyzed. The first category included heavy metals (As, Cd, Pb, Hg, Cr, Ni, Cu, and Zn), while the second category included water quality indicators, namely COD, TN, and TP. Specifically, heavy metals were determined in accordance with HJ 677–2013, Water Quality—Digestion of Total Metals—Nitric Acid Digestion Method;[27] COD was determined in accordance with HJ/T 399–2007, Water Quality—Determination of the Chemical Oxygen Demand—Fast Digestion-Spectrophotometric Method;[28] TN was determined in accordance with HJ 636–2012, Water Quality—Determination of Total Nitrogen—Alkaline Potassium Persulfate Digestion UV Spectrophotometric Method;[29] and TP was determined in accordance with GB 11893–89, Water quality—Determination of Total Phosphorus—Ammonium Molybdate Spectrophotometric Method,[30] respectively. The measured concentrations were compared to the relevant national standards to evaluate the environmental safety of the SS. In addition, the effect of curing atmosphere on pollutant release was investigated by comparing the leaching behavior of air-cured and anaerobically cured specimens. Three parallel specimens were prepared for each group, and the average values were used for analysis.

2.6. Microstructural characterization

Raw sediment, CA–SS, and CA–BC–SS for seven days were selected for microscopic characterization using XRD, FTIR, and SEM. For XRD and FTIR analyses, samples were taken from the inner portion of the UCS specimens, oven-dried at 40 °C for more than 48 h, ground into a powder, and passed through a 0.075 mm sieve. XRD analysis was performed using an X-ray diffractometer (D8 Advance, Bruker, USA), while FTIR spectra were collected using a Fourier transform infrared spectrometer (Nicolet iS20, Thermo Fisher Scientific, USA). For SEM observation, intact portions of the UCS specimens were cut into cubes of approximately 1 cm^3 and dried at 40 °C for more than 48 h. The dried specimens were then fractured to expose fresh surfaces, sputter-coated with gold, and examined using a field emission scanning electron microscope (JSM-7610F, JEOL, Japan).

3. Results and discussion

3.1. Optimization of solidification conditions

3.1.1. Effect of initial water content and mayenite dosage on unconfined compressive strength

The UCS of SS under different initial water contents and CA dosages is presented in Figure 1. A similar trend was observed across all CA dosages, with UCS increasing initially and then decreasing as the initial water content increased. Regardless of moisture content, increasing the CA dosage from 25% to 40% markedly improved UCS, whereas further increases to 45–50% provided only limited additional strength gain.

The initial water content played a critical role in the stabilization performance. As moisture content increased from 40% to 70%, UCS increased continuously, suggesting that an appropriate amount of water promoted CA dispersion and facilitated hydration. However, when the moisture content was further increased to 80%, the UCS decreased because excess pore water reduced the compactness of the stabilized matrix. A similar trend was observed with CA dosage. Increasing the dosage supplied more reactive material for hydration and enhanced strength development, whereas the improvement became marginal beyond 40%, indicating that the effectiveness of additional CA gradually diminished under the investigated conditions.

The highest UCS (0.45 ± 0.02 MPa) was achieved at an initial water content of 70% with a 40% CA dosage. These conditions were therefore selected as the optimum baseline for the subsequent optimization of the CA–BC composite stabilization system.

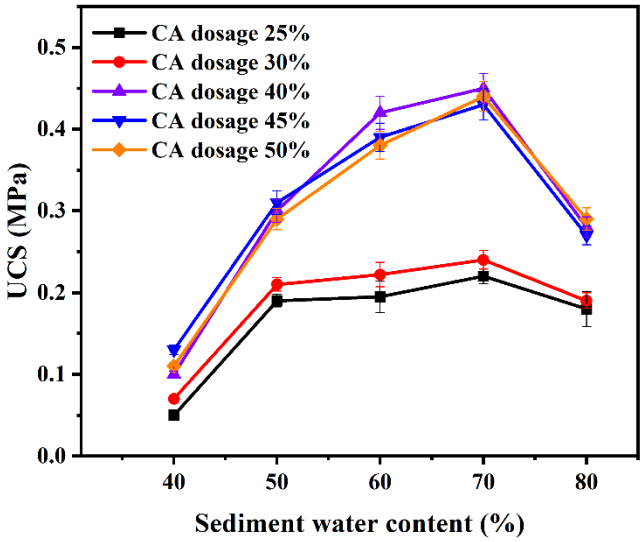

Figure 1. Effect of initial sediment water content and mayenite (CA) dosage on the unconfined compressive strength (UCS) of stabilized sediment after seven days of curing

3.1.2. Effect of mayenite particle size on unconfined compressive strength

The effect of CA particle size on the UCS of SS was evaluated under the optimized conditions of 70% initial water content and 40% CA dosage. The results are shown in Figure 2. As the CA particle size decreased from 100 mesh to 250 mesh, UCS increased from 1.22 ± 0.02 MPa to 1.81 ± 0.06 MPa, a 48.4% increase. Further refinement to 300 mesh slightly decreased UCS to 1.70 ± 0.08 MPa, indicating that particle size had a non-monotonic influence on strength development.

The improved UCS with finer CA particles is likely due to their larger specific surface area, which enhanced contact with sediment particles and promoted hydration reactions. Consequently, more hydration products were generated, leading to a denser and stronger stabilized matrix. However, reducing the particle size beyond 250 mesh did not further improve the UCS, suggesting that the beneficial effect of particle refinement reached an optimum under the present conditions. Therefore, 250-mesh CA was selected for the subsequent investigation of the CA–BC composite stabilization system.

3.1.3. Effect of coconut shell biochar dosage on unconfined compressive strength

The effect of BC dosage on the UCS of SS was evaluated under the optimized conditions for the CA-only system (70% initial water content, 40% CA, and 250-mesh CA). The corresponding results are presented in Figure 3. The UCS increased with increasing BC dosage and reached a maximum value of 2.15 ± 0.11 MPa at 20% BC, representing an improvement of approximately 21.5% compared with the CA-only specimen (1.81 ± 0.06 MPa). Further increasing the BC dosage to 25% resulted in a slight decrease in UCS, although the strength remained higher than that of the specimen without BC.

The enhanced strength at moderate BC dosages is likely attributed to the porous structure and large specific surface area of BC, which improved the interaction between hydration products and sediment particles, resulting in a denser composite matrix.[31] However, excessive BC addition did not produce further strength enhancement, indicating the existence of an optimum BC dosage for the CA–BC stabilization system. Based on these results, 20% BC was selected for the subsequent investigation of BC particle size.

3.1.4. Effect of coconut shell biochar particle size on unconfined compressive strength

The effect of BC particle size on the UCS of SS was investigated under the optimized conditions of 70% initial water content, 40% CA, 250-mesh CA, and 20% BC. The results are presented in Figure 4. As the BC particle size decreased from 100 mesh to 200 mesh, the UCS increased from 1.85 ± 0.06 MPa to 2.31 ± 0.11 MPa, corresponding to an increase of 24.5%. Further refinement to 250 and 300 mesh reduced the UCS to 2.19 ± 0.04 MPa and 2.07 ± 0.10 MPa, respectively.

The increase in UCS with decreasing BC particle size can be attributed to the larger specific surface area

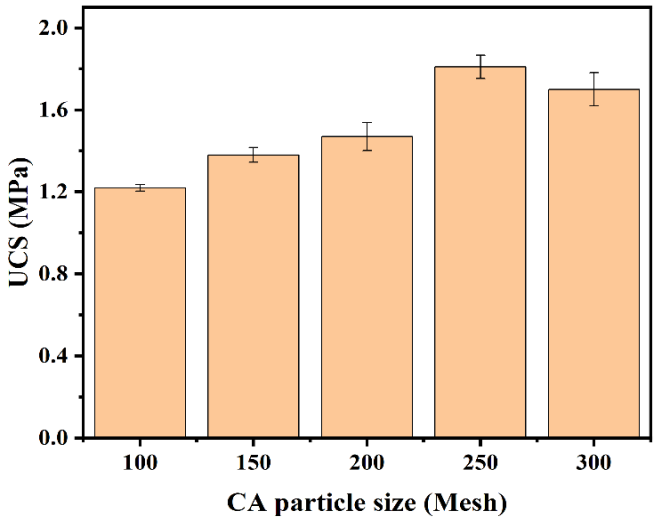

Figure 2. Effect of mayenite (CA) particle size on the unconfined compressive strength (UCS) of stabilized sediment (initial sediment water content of 70%; CA dosage of 40%)

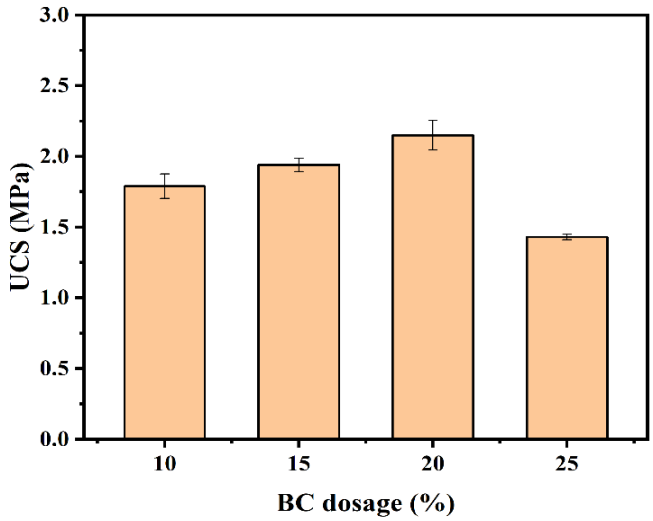

Figure 3. Effect of coconut shell biochar (BC) dosage on the unconfined compressive strength (UCS) of stabilized sediment (initial sediment water content of 70%; mayenite [CA] dosage of 40%; CA particle size of 250 mesh)

of finer BC particles, which enhanced their interaction with hydration products and sediment particles, thereby improving the compactness of the composite matrix. However, further refinement beyond 200 mesh did not provide additional strength enhancement, suggesting that the beneficial effect of BC particle size reached an optimum under the investigated conditions. Consequently, 200-mesh BC was selected for the subsequent microstructural characterization and leaching tests.

Based on the above results, the optimum stabilization formulation consisted of 70% initial water content, 40% CA (250 mesh), and 20% BC (200 mesh). This formulation was adopted for all subsequent microstructural characterization and leaching experiments.

3.2. Microstructure evolution of stabilized sediment

3.2.1. X-ray Diffraction analysis

The XRD patterns of the raw sediment and SSs are presented in Figure 5. The raw sediment was mainly composed of quartz (SiO_2), accompanied by minor amounts of halloysite, kaolinite, muscovite, albite, calcite, and phillipsite. Among these minerals, quartz exhibited

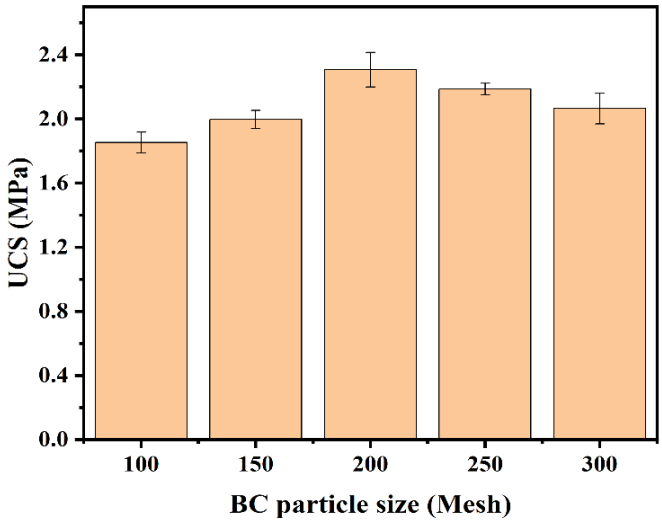

Figure 4. Effect of coconut shell biochar (BC) particle size on the unconfined compressive strength (UCS) of stabilized sediment (initial sediment water content of 70%; mayenite [CA] dosage of 40%; CA particle size of 250 mesh; BC dosage of 20%)

the strongest diffraction peak at 2θ = 26.7°, indicating that it was the dominant crystalline phase in the untreated sediment.[32,33]

Compared to the raw sediment, the mineralogical composition changed noticeably after CA stabilization. After stabilization with CA, noticeable changes occurred in the diffraction patterns. The intensity of the quartz peak decreased, while new diffuse diffraction peaks corresponding to AFt and calcium silicate hydrate (C–S–H, 2θ = 29°~35° and 2θ = 50°~60°) appeared.[19,34] These newly formed hydration products suggest that CA actively participated in hydration reactions instead of acting merely as an inert filler. The formation of AFt and C–S–H likely enhanced interparticle bonding by filling pores and bridging adjacent sediment particles,[35] thereby contributing to the improved UCS.

Increasing the CA dosage from 25% to 40% made the diffraction features of AFt and C–S–H more pronounced, suggesting enhanced hydration under the investigated conditions. However, no obvious new crystalline phases were observed when the CA dosage exceeded 40%, suggesting that further increasing the binder content mainly increased the amount of existing hydration products rather than altering the mineralogical composition. This observation is consistent with the UCS results, where the strength improvement became marginal at CA dosages above 40%.

The XRD pattern of the $CA_{40\%}$–$BC_{20\%}$–SS specimen was generally similar to that of the $CA_{40\%}$–SS specimen, indicating that the incorporation of BC did not introduce additional crystalline phases. No additional crystalline phases were observed after BC incorporation, because biochar is predominantly amorphous and therefore does not exhibit distinct diffraction peaks. Nevertheless, the diffraction peaks corresponding to hydration products remained evident in the composite-stabilized specimen, indicating that CA hydration was not hindered by BC addition. These results suggest that BC mainly contributed by optimizing the internal microenvironment while maintaining the hydration process of CA, rather than generating additional crystalline phases.

3.2.2. Fourier transform infrared spectroscopy analysis

The FTIR spectra of the raw sediment, $CA_{40\%}$–SS, and $CA_{40\%}$–$BC_{20\%}$–SS are presented in Figure 6. The raw sediment exhibited characteristic absorption bands associated with hydroxyl groups and aluminosilicate minerals. The broad band around 3,400 cm^{-1} was attributed to O–H stretching vibrations of adsorbed water and hydroxyl groups, while the bands in the range of 1,000–450 cm^{-1} were mainly related to Si–O and Al–O vibrations.[36] These observations are consistent with the mineralogical composition identified by XRD.

After stabilization with CA, the Si–O and Al–O bands became more pronounced, suggesting that hydration reactions occurred during curing. Combined with the XRD results, the enhanced Si–O and Al–O bands likely reflect the formation of hydration products, including C–S–H and AFt, which contributed to bonding between sediment particles and matrix densification. Compared to

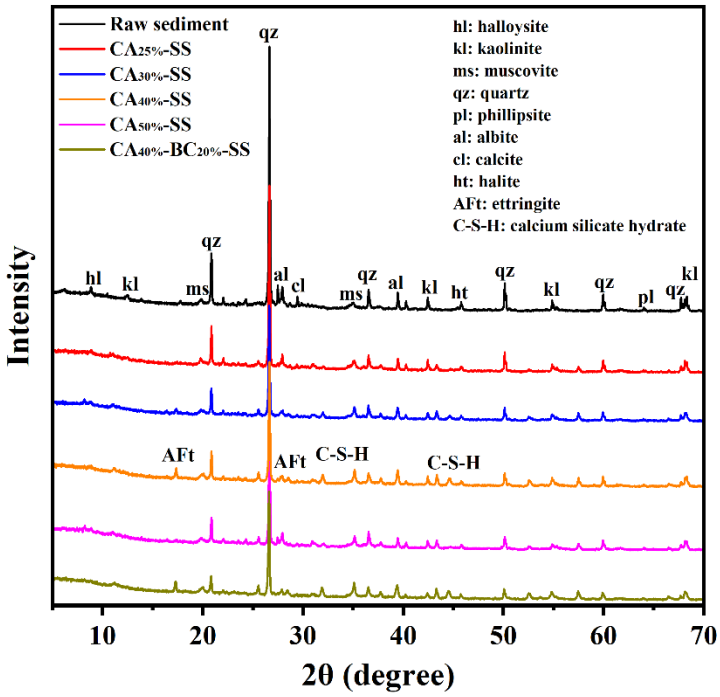

Figure 5. The X-ray diffraction patterns of raw sediment, $CA_{x\%}$–SS, and $CA_{40\%}$–$BC_{20\%}$–SS

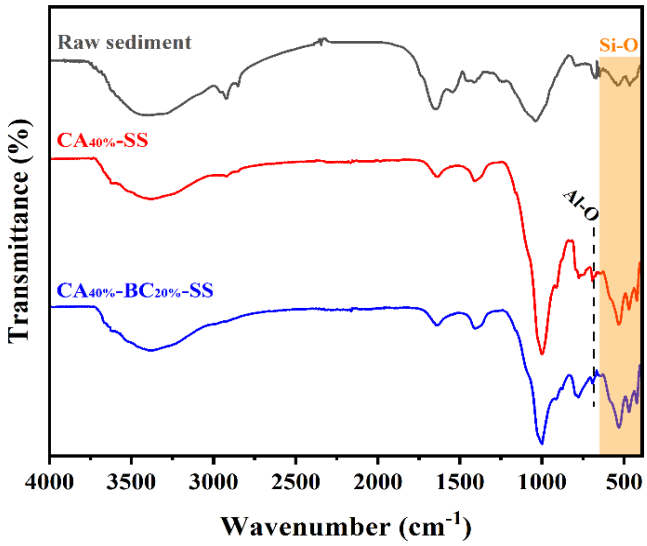

Figure 6. The Fourier transform infrared spectra of raw sediment, $CA_{40\%}$–SS, and $CA_{40\%}$–$BC_{20\%}$–SS

$CA_{40\%}$–SS, the FTIR spectrum of $CA_{40\%}$–$BC_{20\%}$–SS exhibited similar characteristic bands without the appearance of new functional groups, suggesting that BC incorporation did not introduce obvious changes in the characteristic hydration-related bands. Since biochar is predominantly amorphous, it generally does not produce distinct characteristic peaks in FTIR spectra.[37] The enhanced Si–O and Al–O signals in the composite-SS suggest that BC addition was compatible with CA hydration and may have promoted the development of a denser cemented structure through optimization of the internal microenvironment. These observations are consistent with the XRD and UCS results, supporting the synergistic stabilization effect of the CA–BC composite system.

3.2.3. Scanning electron microscopy analysis

The SEM images of the raw sediment, synthesized CA, CA–SS, and CA–BC–SS are presented in Figure 7. As shown in Figure 7A, the raw sediment exhibited a loose and heterogeneous microstructure composed of irregular fine particles with weak interparticle contacts and abundant open pores. The particles were mainly dispersed or flocculated, and no continuous load-bearing framework was observed. Such a loose and porous microstructure is consistent with the low UCS and poor engineering stability of the raw sediment.[38] The as-synthesized CA (Figure 7B) consisted of agglomerated nanoparticles with an irregular porous morphology, which agrees well with the morphology of $Ca_{12}Al_{14}O_{33}$ reported by Ruttanapun *et al.*[39]

The SEM images of the sediments stabilized with 30% and 40% CA are shown in Figure 7C–F, respectively. Distinct microstructural evolution was observed after CA stabilization. Compared to the raw sediment, both stabilized specimens exhibited markedly denser microstructures with substantially fewer open pores and improved particle contacts. Numerous gel-like amorphous hydration products were observed throughout the matrix. Combined with the XRD identification of hydration products, these gel-like phases were mainly associated with C–S–H gel.[40] As the CA dosage increased from 30% to 40%, the amount of hydration products increased noticeably, while the pore volume decreased substantially. The newly formed hydration products bridged adjacent sediment particles and progressively filled the pore spaces, resulting in a more continuous cemented framework. Consequently, the $CA_{40\%}$–SS specimen exhibited a more compact microstructure, which is consistent with its significantly higher UCS.

The SEM images of the $CA_{40\%}$–$BC_{20\%}$–SS are presented in Figure 7G and 7H. Compared with $CA_{40\%}$–SS, incorporating BC further refined the microstructure, resulting in a denser, more homogeneous matrix with fewer visible interconnected pores. Abundant light-colored amorphous flocculent phases were distributed around and partially coated the sediment particles, while the particle interfaces became more continuous and compact. No distinct BC particles were observed in the SEM images, suggesting that BC was well dispersed within the matrix and closely associated with the surrounding hydration products, indicating good interfacial compatibility. Rather than acting as an independent cementitious phase, BC mainly optimized the pore structure and promoted a more uniform distribution of the solid phase, contributing to the formation of a denser stabilized matrix. The corresponding EDX analysis (Figure 8) showed that $CA_{40\%}$–$BC_{20\%}$–SS mainly contained O (46.1 at.%), Si (15.5 at.%), Al (12.4 at.%), and Ca (12.3 at.%). The coexistence of Ca, Si, Al, and O is consistent with the composition of calcium silicate hydrate (C–S–H) and/or calcium aluminum silicate hydrate (C–A–S–H).[41] Combined with the XRD results, these findings confirm the formation of hydration products responsible for particle bonding and matrix densification. The denser microstructure explains the higher UCS and the improved contaminant immobilization achieved by the CA–BC–SS.

The SEM observations are consistent with the XRD, FTIR, and UCS results. CA hydration generated abundant cementitious products that bonded sediment particles and reduced pore volume through progressive pore filling, whereas BC further refined the pore structure and improved matrix homogeneity. These microstructural changes provide direct evidence for the synergistic stabilization mechanism of CA–BC, accounting for the enhanced mechanical performance and reduced contaminant leaching of the SS.

3.3. Leaching behavior

3.3.1. Heavy metal leaching characteristics

The leaching concentrations of heavy metals from the raw sediment, $CA_{40\%}$–SS, and $CA_{40\%}$–$BC_{20\%}$–SS are summarized in Table 2. The measured values were compared with the leachate limits specified in *Identification Standards for Hazardous Wastes-Identification for Extraction Toxicity* (GB 5085.3–2007)[42] to evaluate the environmental safety of the SSs.

The raw sediment exhibited relatively high leaching concentrations of several heavy metals, particularly Zn (10.7 mg/L), Cu (7.69 mg/L), Ni (4.81 mg/L), Cr (4.03 mg/L), As (2.49 mg/L), and Pb (2.24 mg/L), indicating considerable environmental risk. After stabilization with 40% CA, the leaching concentrations of all investigated metals decreased markedly. The removal efficiencies reached 99.9% (As), 99.1% (Cd), 99.9% (Pb), 70.0% (Hg), 98.4% (Cr), 99.1% (Ni), 97.8% (Cu), and 98.1% (Zn). All measured concentrations were substantially lower than the limits specified in GB 5085.3–2007, demonstrating the excellent immobilization capability of the CA–SS.[42]

Incorporating 20% BC further improved heavy metal immobilization. Compared with the CA-only specimen, the leaching concentrations of As, Hg, Cr, Ni, Cu, and Zn were further reduced by 33.3%, 16.7%, 46.9%, 25.6%, 79.2%, and 98.5%, respectively, while Cd and Pb were below the detection limit. The most significant improvement was observed for Zn, whose concentration decreased from 0.202 mg/L to 0.003 mg/L after BC addition. These results indicate that BC effectively enhanced the immobilization performance of the CA stabilization system.

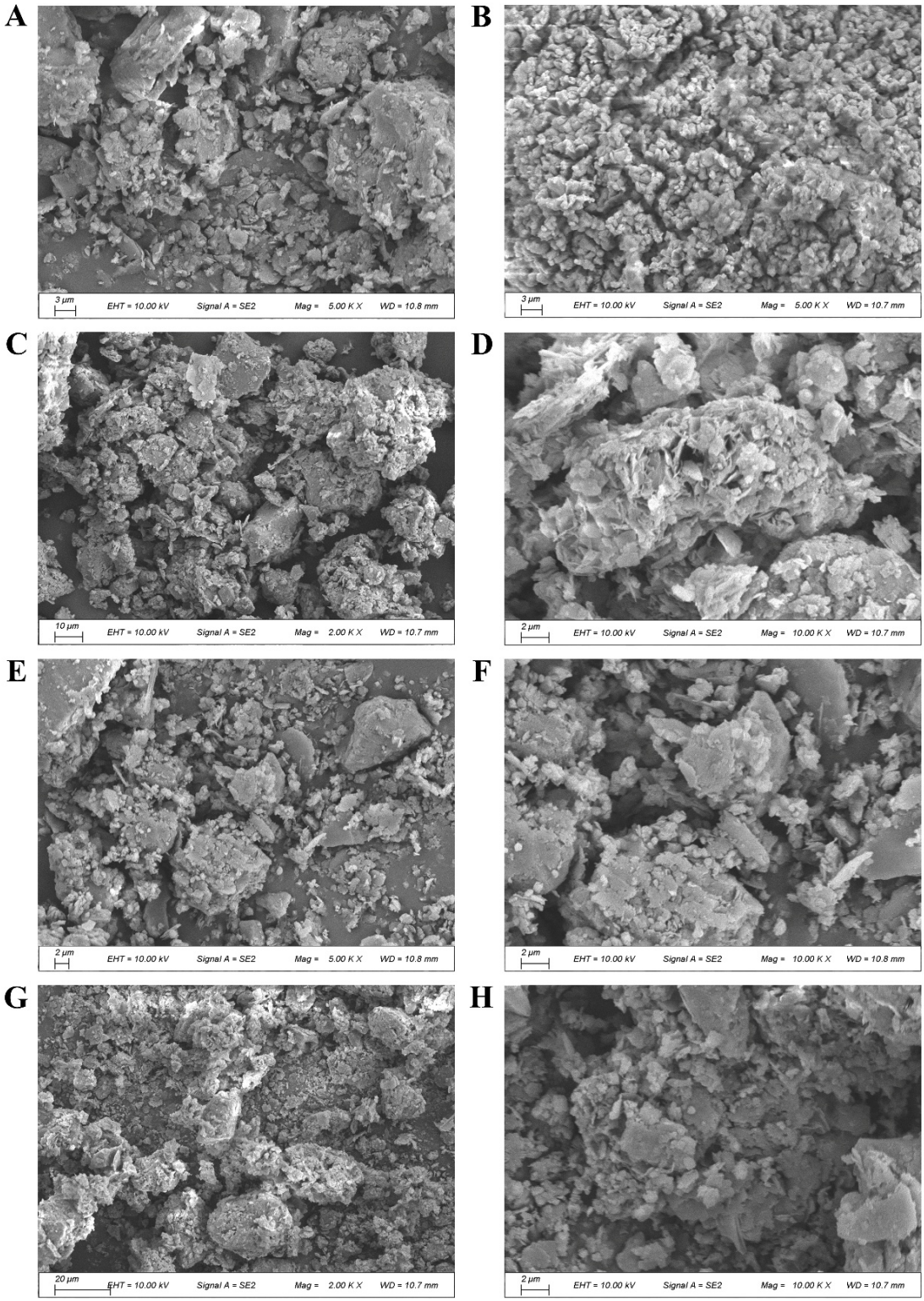

Figure 7. The scanning electron microscopy images of: (A) Raw sediment. Scale bar: 3 µm; magnification: 5,000×. (B) As-synthesized CA. Scale bar: 3 µm; magnification: 5,000×. (C, D) $CA_{30\%}$–SS. Scale bars: 2 µm, 10 µm; magnifications: 10,000×, 2,000×. (E, F) $CA_{40\%}$–SS. Scale bar: 2 µm; magnifications: 5,000×, 10,000×. (G, H) $CA_{40\%}$–$BC_{20\%}$–SS. Scale bars: 2 µm, 20 µm; magnifications: 10,000×, 2,000×.

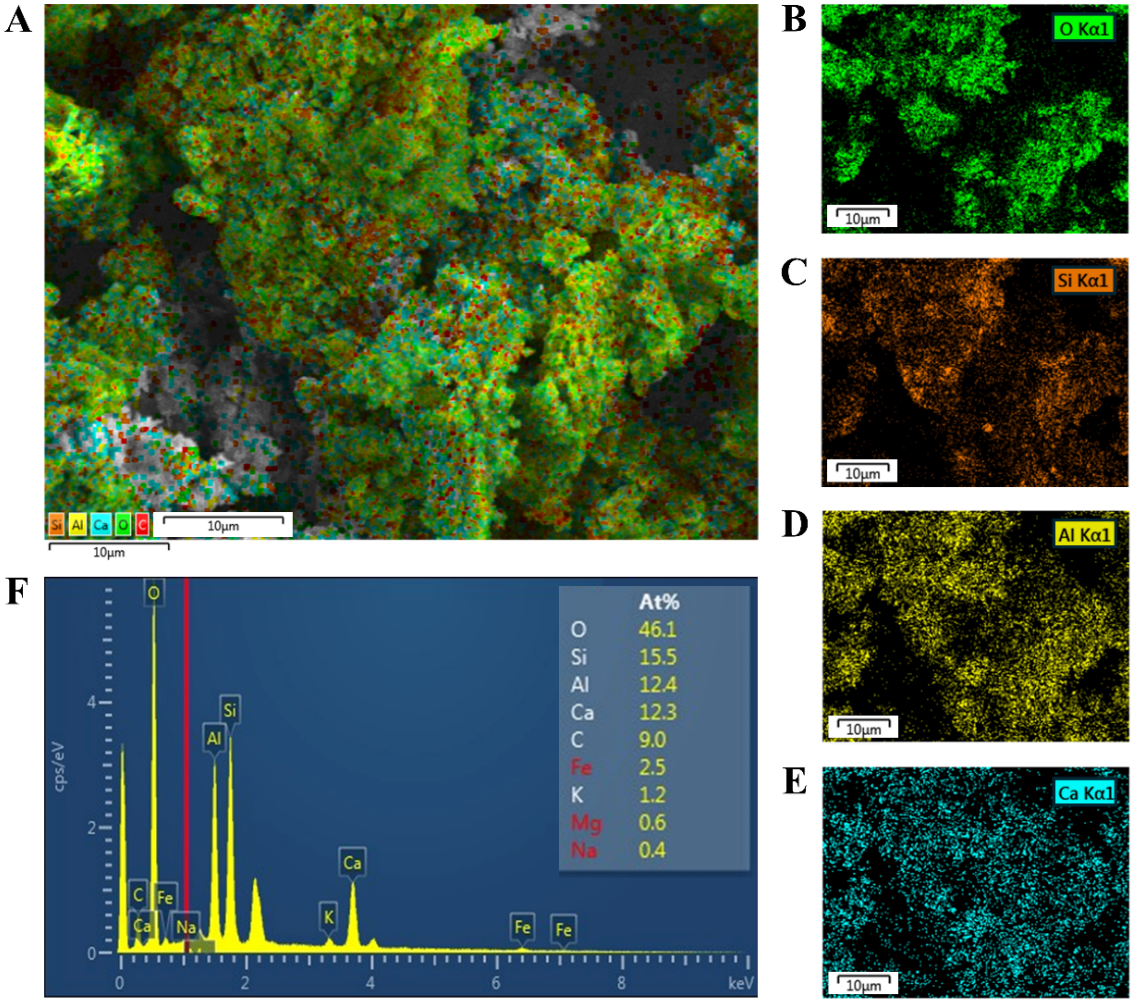

Figure 8. The scanning electron microscopy–energy-dispersive X-ray spectroscopy mapping of $CA_{40\%}$–$BC_{20\%}$–SS. (A) Elemental overlap image. Scale bar: 10 μm; magnification: 5,000×. (B–E) Distribution maps of O, Si, Al, and Ca elements. Scale bar: 10 μm; magnification: 5,000×. (F) Full surface scanning.

The improved immobilization performance can be attributed to the combined effects of hydration cementation and pore refinement. As shown by XRD, SEM, and EDX analyses, CA hydration generated abundant cementitious products, including C–S–H, which bound sediment particles into a denser matrix and reduced pore connectivity. Incorporating BC further optimized pore structure and matrix homogeneity while providing additional adsorption sites for dissolved metal ions through its porous structure and surface functional groups. Consequently, contaminant migration was effectively suppressed. These results indicate that incorporating BC not only enhances the mechanical strength of CA–SS but also substantially improves its environmental compatibility, thereby facilitating sustainable resource utilization of dredged sediment in geotechnical engineering applications.

3.3.2. Leaching characteristics of chemical oxygen demand, total nitrogen, and total phosphorus

The leaching concentrations of COD, TN, and TP under different curing conditions are summarized in Table 3. Compared with the raw sediment, both CA and CA–BC stabilization markedly reduced the release of organic matter and nutrients.

Under air-curing conditions, leaching concentrations of COD, TN, and TP decreased from 5.04, 28.7, and 2.23 mg/L in the raw sediment to 1.52, 0.039, and 0.012 mg/L after CA stabilization, corresponding to reductions of 69.8%, 99.9%, and 99.5%. After incorporating 20% BC, TN and TP decreased further to 0.034 and 0.010 mg/L, respectively, while COD remained similarly low (1.72 mg/L). Under anaerobic curing, pollutant release

Table 2. Heavy metal leaching concentrations of raw sediment and SSs, and the corresponding regulatory limits (unit: mg/L)

Heavy metal	Leaching concentration of raw sediment	Leaching concentration of specimen		Leachate limit value (in accordance with GB 5085.3–2007)
		$CA_{40\%}$–SS	$CA_{40\%}$–$BC_{20\%}$–SS	
Total As	2.49 ± 0.10	0.003 ± 0.0001	0.003 ± 0.0001	5.00
Total Cd	0.11 ± 0.00	0.001 ± 0.000	Not detected	1.00
Total Pb	2.24 ± 0.09	0.002 ± 0.0001	Not detected	5.00
Total Hg	0.02 ± 0.00	0.006 ± 0.0002	0.006 ± 0.0002	0.100
Cr(VI)	4.03 ± 0.16	0.064 ± 0.0026	0.034 ± 0.0014	5.00
Total Ni	4.81 ± 0.19	0.043 ± 0.0017	0.032 ± 0.0013	5.00
Total Cu	7.69 ± 0.31	0.168 ± 0.0067	0.035 ± 0.0014	100.0
Total Zn	10.7 ± 0.43	0.202 ± 0.0081	0.003 ± 0.0001	100.0

Abbreviations: BC: Coconut shell biochar; CA: Mayenite; SS: Stabilized sediment.

remained substantially lower than in the raw sediment but consistently higher than under air curing. For example, the COD, TN, and TP concentrations of $CA_{40\%}$–$BC_{20\%}$–SS increased from 1.72, 0.034, and 0.010 mg/L under air curing to 2.37, 0.056, and 0.015 mg/L, respectively, under anaerobic curing.

The reduced pollutant release is attributed to the combined effects of hydration products and microstructural densification. As confirmed by the XRD, FTIR, and SEM results, CA hydration generated a continuous cemented matrix that restricted contaminant diffusion, while BC further refined the pore structure and provided additional adsorption sites for dissolved organic matter and nutrient species. Consequently, the CA–BC composite exhibited superior control of TN and TP leaching compared with CA alone. Moreover, air curing consistently resulted in lower pollutant release than anaerobic curing, suggesting that aerobic conditions produced a more stable cemented structure. Collectively, these findings demonstrate that the CA–BC composite effectively enhances both the engineering performance and environmental stability of SS.

3.4. Stabilization mechanism

Based on the mechanical performance, leaching behavior, and microstructure characterization results, the stabilization mechanism of the CA–BC composite can be attributed to the synergistic effects of hydration cementation, structural densification, pore refinement, and contaminant immobilization, as schematically illustrated in Figure 9. In this composite system, CA primarily governs the mechanical stabilization of the sediment, whereas BC mainly contributes to environmental stabilization through pore regulation and adsorption-assisted contaminant retention.

After incorporation into the high-water-content sediment, CA acts as the primary reactive component and establishes the structural foundation of the stabilized matrix. Through hydration reactions, CA generates cementitious phases, mainly C–S–H and AFt, which progressively bind sediment particles, fill interparticle voids, and construct a continuous load-bearing framework. Meanwhile, fine CA particles improve particle packing and reduce structural defects, resulting in a denser matrix with enhanced stress transfer capability. These processes drive the significant improvement in UCS and the transition of the sediment from a weak, loose structure to a mechanically stable cemented body.

In contrast, BC mainly enhances the environmental stability of the SS by optimizing the internal microstructure and providing additional retention sites for pollutants. The porous structure and abundant surface functional groups of BC facilitate the adsorption and immobilization of dissolved organic matter, nutrients, and heavy metal ions, while its incorporation further refines the pore network and reduces the accessibility of transport pathways. Therefore, BC is not the primary cementitious phase but a functional modifier that improves the microenvironment of the CA-based matrix and strengthens resistance to pollutant migration.

Through the complementary roles of CA and BC,

Table 3. Leaching concentrations of pollution indicators of raw sediment and SS curing in air and anaerobic conditions (unit: mg/L)

Indicators	Raw sediment		Leaching concentration of $CA_{40\%}$–SS		Leaching concentration of $CA_{40\%}$–$BC_{20\%}$–SS	
	Total concentration (mg/kg)	Leaching concentration	Air curing	Anaerobic curing	Air curing	Anaerobic curing
TN	272 ± 13.6	28.7 ± 1.15	0.039 ± 0.002	0.071 ± 0.0028	0.034 ± 0.0007	0.056 ± 0.0011
TP	95.4 ± 3.77	2.23 ± 0.09	0.012 ± 0.001	0.019 ± 0.0003	0.010 ± 0.0004	0.015 ± 0.0002
COD	27.5 ± 1.38	5.04 ± 0.12	1.52 ± 0.011	1.70 ± 0.026	1.72 ± 0.047	2.37 ± 0.026

Abbreviations: BC: Coconut shell biochar; CA: Mayenite; COD: Chemical oxygen demand; SS: Stabilized sediment; TN: Total nitrogen; TP: Total phosphorus.

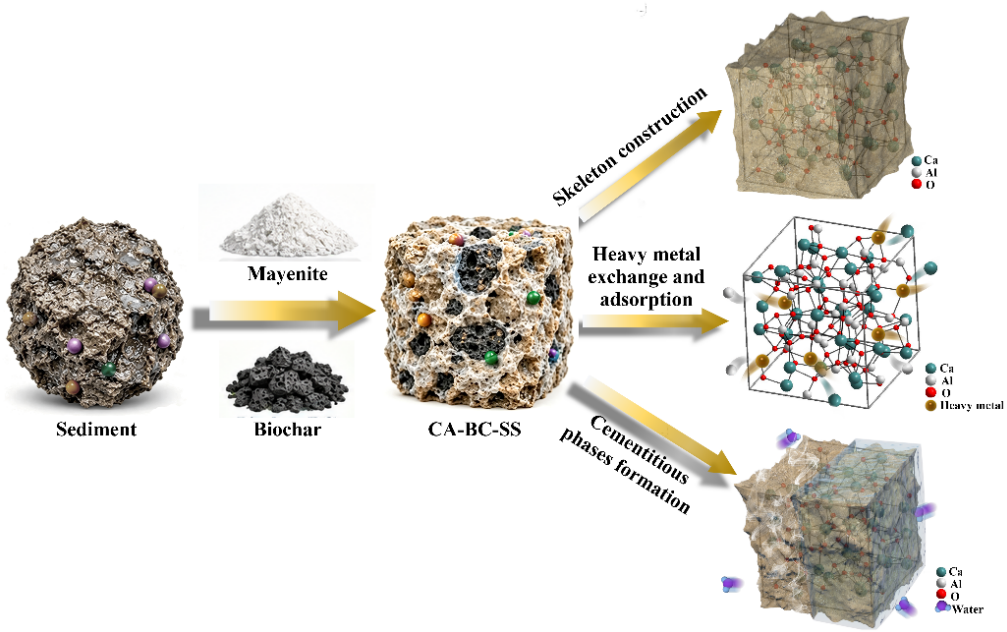

Figure 9. Schematic illustration of the stabilization mechanism

the composite system achieves a dual enhancement of mechanical performance and environmental safety. CA provides the dominant cementation and structural reinforcement required for strength development, whereas BC enhances contaminant immobilization and long-term environmental stability. The combined effects of hydration bonding, pore refinement, physical encapsulation, and adsorption retention form a compact, stable sediment matrix with improved engineering properties and reduced environmental risks. This synergistic stabilization mechanism highlights the potential of the CA–BC composite as an effective strategy for the sustainable treatment and resource utilization of dredged urban river sediments.

4. Conclusion

This study developed a CA–BC composite stabilization strategy for urban river sediments and systematically evaluated its mechanical performance, microstructural evolution, and environmental safety. The main conclusions are as follows:

(i) The incorporation of CA significantly improved the mechanical performance of the SS, while the addition of BC further enhanced the overall stabilization effect. The optimum condition was identified as an initial water content of 70%, 40% CA with a particle size of 250 mesh, and 20% BC with a particle size of 200 mesh, under which the SS achieved a maximum UCS

of 2.31 ± 0.11 MPa. These results indicate that both binder dosage and particle size play important roles in determining the stabilization efficiency of the CA–BC composite.

(ii) The mechanical improvement of the CA–BC–SS was mainly attributed to the synergistic effects of hydration cementation and pore-structure regulation. The hydration of CA generated cementitious products, mainly C–S–H and AFt, which bonded sediment particles and progressively formed a denser and more continuous load-bearing framework. Meanwhile, BC refined pores and homogenized the matrix, providing additional physical support and adsorption sites within the stabilized matrix.

(iii) The CA–BC composite exhibited superior environmental stabilization compared with CA alone, as reflected by the reduced leaching concentrations of heavy metals, COD, TN, and TP. This enhanced immobilization mainly resulted from the combined effects of physical encapsulation and adsorption-assisted contaminant retention.

In brief, the stabilization mechanism of the CA–BC system involved the synergistic effects of hydration cementation, pore regulation, physical encapsulation, and adsorption-assisted immobilization, demonstrating its potential for the safe and resource-oriented utilization of urban river sediments. This study provides a feasible, sustainable approach to dredged sediment stabilization and offers practical guidance for developing low-carbon composite binders.

Acknowledgments

None.

Funding

This work was supported by the Scientific Research Project of China Three Gorges Corporation (NBWL202300013) and the National Natural Science Foundation of China (22306078).

Conflict of interest

The authors declare they have no competing interests.

Author contributions

Conceptualization: Wenhao Li, Dongdong Ge
Data curation: Haoyuan Zhang, Yalin Yu
Formal analysis: Ning Fang, Xiankai Wang
Investigation: Haoyuan Zhang, Ning Fang, Xiankai Wang
Methodology: Wenhao Li, Shouqiang Huang, Dongdong Ge
Supervision: Wenhao Li, Dongdong Ge
Writing–original draft: Wenhao Li, Yalin Yu
Writing–review & editing: Yalin Yu, Haoyuan Zhang, Dongdong Ge

Availability of data

The data presented in this study are available from the corresponding author upon reasonable request.

References

1. Beljin J, Slijepčević N, Duduković N, Tomašević Pilipović D. Sediment pollution: unraveling its impact on water quality, resource management and navigating towards sustainable development goals. *Int J Environ Sci Technol*. 2026;23:525.

   doi: 10.1007/s13762-026-07329-4

2. Mahfoud E, Ndiaye K, Maherzi W, Aggoun S, Benzerzour M, Abriak N-E. Mechanical properties and shrinkage performance of one-part-geopolymer based on fly ash and micronized dredged sediments. *Dev Built Environ*. 2023;16:100253.

   doi: 10.1016/j.dibe.2023.100253

3. Zhang Z, Cui Y, Ma J, *et al*. Analysis and prospect of treatment measures for black-odorous water sediment in China. *E3S Web Conf*. 2020;194:04005.

   doi: 10.1051/e3sconf/202019404005

4. Chen Z, You N, Chen C, Zhang Y. Properties of dredged sludge solidified with alkali-activated slag-based materials and blended with copper slag as fine aggregates of mortars. *Constr Build Mater*. 2021;312:125459.

   doi: 10.1016/j.conbuildmat.2021.125459

5. Wang S, He X, Cai G, *et al*. Strength characteristic and micro-mechanism of organic dredged sludge solidified by cement incorporating sodium persulfate. *Dev Built Environ*. 2024;17:100323.

   doi: 10.1016/j.dibe.2024.100323

6. Zheng W, Yu J, Cai Y, Weng Z. Evaluating the engineering performance and mechanisms of sodium lignosulfonate-modified mineral cementitious materials in fluidized solidified coastal sediment. *Constr Build Mater*. 2026;514:145563.

   doi: 10.1016/j.conbuildmat.2026.145563

7. Wang H, Ding Y, Dong L, Wang D, Sun D, Yan F. Solidified high moisture and high organic content sediment as liquefied backfill material for urban underground space. *Acta Geotech*. 2026.

   doi: 10.1007/s11440-026-02960-4

8. Feng J, Yu Y, Huang S, Zhu N, Mojiri A, Ge D. Tannic acid as a green chemical for the removal of various heavy metals: A critical review of recent developments. *J Environ Manage*. 2025;375:124390.

doi: 10.1016/j.jenvman.2025.124390

9. Wang J, Wang H, Ding J, Ni J, Mou C, Wan X. Investigation on performance improvement of dredged sediment with high water content stabilized with alkali-activated materials. *J Soils Sediments*. 2024;24(3):1464-1473.

   doi: 10.1007/s11368-023-03680-y

10. Cino CM, Petrella A, Todaro F, Notarnicola M. Recycling of marine sediments in cement-based materials by stabilization/solidification treatment: Effect on the mechanical and microstructural properties. *Recycling*. 2025;10(5):169.

    doi: 10.3390/recycling10050169

11. Mastoi AK, Alidekyi SN, Ali M, Channa IA, Dahri AA, Khan U. Effect of flocculant and Tartaric acid on solidification behavior of GGBS-MgO solidified dredged slurry treated with chemical-physical combined method. *Int J Environ Sci Technol*. 2025;22(14):14173-14184.

    doi: 10.1007/s13762-025-06550-x

12. Zhao C, Sun Y, Wu Z, Lv J, Peng D, Meng C. Calcium silicate hydrate-mediated in-situ phosphorus immobilization facilitates subsequent eutrophic sediment dewatering through structure reorganization. *Chem Eng J*. 2026;535:175573.

    doi: 10.1016/j.cej.2026.175573

13. Yu Y, Feng J, Zhu N, Ge D. Ferric tannate-enhanced electrochemical conditioning process for improving sludge dewaterability. *Water*. 2025;17(16):2424.

    doi: 10.3390/w17162424

14. Wu R, Liu Y, Zhang S, *et al*. Characterization of nitrogen and phosphorus at the ice-water-sediment interface and the effect of their migration on overlying water quality in Daihai Lake (China) during the freezing period. *Sci Total Environ*. 2023;893:164863.

    doi: 10.1016/j.scitotenv.2023.164863

15. Xu Q, Wu B, Chai X. In situ remediation technology for heavy metal contaminated sediment: A review. *Int J Environ Res Public Health*. 2022;19(24):16767.

    doi: 10.3390/ijerph192416767

16. Wang H, Zentar R, Wang D, Ouendi F. New applications of ordinary portland and calcium sulfoaluminate composite binder for recycling dredged marine sediments as road materials. *Int J Geomech*. 2022;22(6):04022068.

    doi: 10.1061/(ASCE)GM.1943-5622.0002373

17. Arairo W, Hamd W, Al Sahmarany B, Ghannoum M, Affan H, Barraj F. Influence of lime stabilization and natural fiber reinforcement on the performance of sediment-based blocks for sustainable construction. *Discov Sustain*. 2026;7:1299.

    doi: 10.1007/s43621-026-03724-6

18. Zhou S, Zhang H, Lv J, *et al*. Valorization of dredged sediment through Al3+-mediated C–A–S–H gel networks: Bridging mechanisms for enhanced structural bonding in non-autoclaved brick production. *J Environ Chem Eng*. 2025;13(5):118681.

    doi: 10.1016/j.jece.2025.118681

19. Deng Y, Yue Z, Wang Z, Huang Q, Yang X. Optimization and mechanism of the novel eco-friendly additives for solidification and stabilization of dredged sediment. *Environ Sci Pollut Res*. 2024;31(17):25964-25977.

    doi: 10.1007/s11356-024-32865-2

20. Cai G-H, Zhou Y-F, Poon CS, Li J-S. Engineering performance and microstructure characteristics of natural marine sediment stabilized with quicklime-activated GGBS under different lime proportions. *Mar Georesour Geotechnol*. 2023;41(8):858-872.

    doi: 10.1080/1064119X.2022.2105765

21. Lourenço RR, Angélica RS, Rodrigues JDA. Preparation of refractory calcium aluminate cement using the sonochemical process. *Mater Res*. 2013;16(4):731-739.

    doi: 10.1590/S1516-14392013005000041

22. Luo J, Cai Y, Yu J, Huang J, Yan J, Zhu Y. A laboratory evaluation of enhanced stabilization of dredged heavy metal-contaminated coastal sediments using a green biochar-metakaolin-sodium silicate composite: Performance, mechanisms, and applications. *J Clean Prod*. 2026;566:148542.

    doi: 10.1016/j.jclepro.2026.148542

23. Luo J, Cai Y, Yu J, Huang J, Yan J. Immobilization and stabilization of heavy metals in coastal sediments using polycrystalline silicon-aluminum biochar-based material GBMSS: Mechanisms and performance. *Chem Eng J*. 2025;519:165510.

    doi: 10.1016/j.cej.2025.165510

24. Gu X, Guo P, Li Z, *et al*. A multifunctional coconut shell biochar modified by titanium dioxide for heavy metal removal in water/soil and tetracycline degradation. *J Clean Prod*. 2024;482:144192.

    doi: 10.1016/j.jclepro.2024.144192

25. Ajien A, Idris J, Md Sofwan N, Husen R, Seli H. Coconut shell and husk biochar: A review of production and activation technology, economic, financial aspect and application. *Waste Manag Res*. 2023;41(1):37-51.

    doi: 10.1177/0734242X221127167

26. Ministry of Ecology and Environment of the People's Republic of China. Solid waste-extraction procedure for leaching toxicity-sulphuric acid and nitric acid method (HJ/T 299–2007). Beijing, China: China Environmental Science Press; 2007. Accessed September 2, 2026. https://www.mee.gov.cn/ywgz/fgbz/bz/bzwb/jcffbz/200704/t20070418_102859.shtml

27. Ministry of Ecology and Environment of the People's Republic of China. Water quality–Digestion of total metals–Nitric acid digestion method (HJ 677–2013). Beijing, China: China Environmental Science Press; 2013. Accessed September 2, 2026. https://www.mee.gov.cn/ywgz/fgbz/bz/bzwb/jcffbz/201312/t20131203_264301.htm

28. Ministry of Ecology and Environment of the People's Republic of China. Water quality–Determination of the chemical oxygen demand–Fast digestion-spectrophotometric method (HJ/T 399–2007). Beijing, China: China Environmental Science Press; 2007. Accessed September 2, 2026. https://www.mee.gov.cn/ywgz/fgbz/bz/bzwb/jcffbz/200712/t20071213_114284.htm

29. Ministry of Environmental Protection of the People's Republic of China. Water quality–Determination of total nitrogen–Alkaline potassium persulfate digestion UV spectrophotometric method (HJ 636–2012). Beijing, China: China Environmental Science Press; 2012. Accessed September 2, 2026. https://www.mee.gov.cn/ywgz/fgbz/bz/bzwb/jcffbz/201203/t20120307_224383.shtml

30. Ministry of Ecology and Environment of the People's Republic of China. Water quality–Determination of total phosphorus–Ammonium molybdate spectrophotometric method (GB 11893–89). Beijing, China: China Environmental Science Press; 1989. Accessed September 2, 2026. https://openstd.samr.gov.cn/bzgk/std/newGbInfo?hcno=E3834D3D19D975F69C69CB359BCB762E

31. Gupta S, Kua HW. Carbonaceous micro-filler for cement: Effect of particle size and dosage of biochar on fresh and hardened properties of cement mortar. *Sci Total Environ*. 2019;662:952-962.

doi: 10.1016/j.scitotenv.2019.01.269

32. Zhu Y, Chen S, Zhong F, *et al*. Solidified dredged sediment as ecological restoration substrate: mechanical strength, water stability, and vegetation performance. *J Soils Sediments*. 2026;26(1):12.

doi: 10.1007/s11368-025-04223-3

33. Ma Q, Wang K, Li Q, Zhang Y. Alkali-activated dredged-sediment-based fluidized solidified soil: Early-age engineering performance and microstructural mechanisms. *Materials*. 2025;18(14):3408.

doi: 10.3390/ma18143408

34. Wang H, Zhang J, Sun D, Li Y, Shi Y. Sustainable solidification/stabilization of high-moisture dredged sediment using solid waste-based cementitious materials blended with OPC: Strength, environmental impact, and micro-mechanism. *J Environ Chem Eng*. 2026;14(3):122347.

doi: 10.1016/j.jece.2026.122347

35. Shi Y, Zhang S, Gao P, Xie W, Wang C, Chen B. Reaction mechanism regulation in high-phosphogypsum supersulfated cement: Nano-metakaolin–induced formation of a compact AFt/C-(A)-S-H network and immobilization of phosphorus and fluorine. *Constr Build Mater*. 2026;512:145347.

doi: 10.1016/j.conbuildmat.2026.145347

36. Zhou H, Zhang H, Zhang Y, *et al*. Solidification/stabilization of composite heavy metal-contaminated soil by red mud-slag-based geopolymer. *J Appl Polym Sci*. 2026;143(35):e71049.

doi: 10.1002/app.71049

37. Pituello C, Francioso O, Simonetti G, *et al*. Characterization of chemical-physical, structural and morphological properties of biochars from biowastes produced at different temperatures. *J Soils Sediments*. 2015;15(4):792-804.

doi: 10.1007/s11368-014-0964-7

38. Zhang J, Yu Y, Li W, *et al*. A novel sludge dewatering conditioner of chitin derivatives from waste black soldier fly puparia: Efficacy, key factors, and mechanisms. *Process Saf Environ Prot*. 2025;202:107789.

doi: 10.1016/j.psep.2025.107789

39. Ruttanapun C, Srepusharawoot P, Maensiri S. Effect of Fe3+-doped Ca12Al14O33 cement on optical and thermal properties. *Chin J Phys*. 2018;56(1):252-260.

doi: 10.1016/j.cjph.2017.12.022

40. Wang L, Tsang D, Poon C. Green remediation and recycling of contaminated sediment by waste-incorporated stabilization/solidification. *Chemosphere*. 2015;122:257-264.

doi: 10.1016/j.chemosphere.2014.11.071

41. Sun Z, Chen W, Zhao R, Jin Y, Yin J. Solidification/stabilization treatment of Hong Kong marine deposits slurry at high water content by ISSA and GGBS. *Constr Build Mater*. 2023;372:130817.

doi: 10.1016/j.conbuildmat.2023.130817

42. State Environmental Protection Administration of China, General Administration of Quality Supervision, Inspection and Quarantine of the People's Republic of China. Identification standards for hazardous wastes–Identification for extraction toxicity (GB 5085.3–2007). Beijing, China: China Environmental Science Press; 2007. Accessed September 2, 2026. https://www.mee.gov.cn/ywgz/fgbz/bz/bzwb/gthw/wxfwjbffbz/200705/t20070522_103957.shtml